Applied Catalysis B: Environmental 224 (2018) 602–611

Contents lists available at ScienceDirect

Applied Catalysis B: Environmental

journal homepage: www.elsevier.com/locate/apcatb

Research Paper

New understandings of ethanol oxidation reaction mechanism on Pd/C and Pd_2Ru/C catalysts in alkaline direct ethanol fuel cells

Junsong Guo[a], Rongrong Chen[b,*], Fu-Chun Zhu[c], Shi-Gang Sun[c], Hebe M. Villullas[d,**]

[a] Richard G. Lugar Center for Renewable Energy, Indiana University Purdue University, Indianapolis, IN 46202, USA
[b] Department of Chemical Engineering, University of Toledo, OH 43606, USA
[c] State Key Laboratory of Physical Chemistry of Solid Surfaces, Department of Chemistry, College of Chemistry and Chemical Engineering, School of Energy Research, Xiamen University, Xiamen, 361005, China
[d] Universidade Estadual Paulista (UNESP), Instituto de Química, 14800-900 Araraquara, SP, Brazil

ARTICLE INFO

Keywords:
Ethanol electro-oxidation
Alkaline direct alcohol fuel cells
Catalyst deactivation

ABSTRACT

Ethanol oxidation reaction (EOR) on Pd_2Ru/C and Pd/C catalysts in alkaline media is studied comprehensively by cyclic voltammetry, chronoamperometry, *in situ* FTIR, single fuel cell test and electrochemical impedance spectroscopy measurements. The results show that, as compared to Pd/C, Pd_2Ru/C favors acetaldehyde formation and hinders its oxidation. Based on X-ray absorption data, which evidence that Ru promotes a larger electronic vacancy of the Pd 4d band, it is expected that the formation of adsorbed ethoxy is favored on Pd_2Ru/C and followed by its oxidation to acetaldehyde facilitated by oxygenated species provided by Ru. In contrast, acetaldehyde oxidation is more difficult on Pd_2Ru/C than on Pd/C likely because the adsorption energy of the reactive species is increased. We also show that the performance of Pd_2Ru/C anode in alkaline direct ethanol fuel cell (ADEFC) is initially better but degrades much more rapidly than that with Pd/C anode under the same test conditions. The degradation is demonstrated to result from the accumulation of large amounts of acetaldehyde, which in alkaline media forms dimers by the aldol condensation reaction. The dimers tend to be responsible for blocking the active sites for further ethanol oxidation. This comprehensive study provides new understandings of the roles of Ru in Pd_2Ru/C for EOR in alkaline media, unveils the causes of the performance degradation of fuel cells with Pd_2Ru/C and demonstrates that initial good performances are not necessarily a valid criterion for selecting appropriate anode catalysts for ADEFC applications.

1. Introduction

The Direct Ethanol Fuel Cell (DEFC) is considered one of the most promising electric power sources [1–3] due to several advantages of ethanol fuel over hydrogen, including existing infrastructure for ethanol production from various sources, storage and transportation, high specific energy and wide availability. However, the sluggish kinetics of ethanol oxidation reaction (EOR) and the need to break C—C bond for completing oxidation of ethanol to CO_2 have been major challenges in the development of DEFCs [4–6]. With the advancement in developing anion-exchange membrane materials, there are growing interests in alkaline Direct Ethanol Fuel Cell (ADEFC) technology [7,8]. Compared with proton exchange membrane (PEM) DEFCs, the most significant advantages of ADEFC include: (1) improved kinetics of both anodic ethanol oxidation reactions and catholic oxygen reduction reactions, and (2) a wide range of catalyst materials besides Pt are stable in alkaline media. Consequently, ADEFCs free of the expensive Pt catalyst can be developed.

In ADEFCs, precious metals such as Pt and Pd are commonly used as primary catalysts for EOR [9,10]. Although some other materials such as Au [11–14], Ag [15] and Ni [16] have also been studied as EOR catalysts in alkaline media, the high overpotentials for ethanol oxidation on these materials restrain their utilization in fuel cells due to the low practical cell voltage. In order to increase catalysts performance, Pt and Pd are usually combined with other transition metals [8], such as Ru [17–20], Sn [20–22], Pb [23–25], Au [26,27], Ni [22,28–31], Ag [32,33], Cu [34–37] or Bi [25,38,39], as alloys, deposits or as ad-atoms. Studies of EOR catalytic activities were also performed for Pt and Pd supported on different carbon materials [40–42] and on various metal oxides and on hybrid supports [43–46]. Furthermore, the EOR activities on Pd/C catalysts have been demonstrated to be higher than that on Pt/C in alkaline media [47]. Now Pd and Pd-based catalysts are widely

* Corresponding author at: Department of Chemical Engineering, The University of Toledo, Ohio 43606, USA.
** Corresponding author at: UNESP, Brazil.
E-mail addresses: Rongrong.Chen@UToledo.Edu (R. Chen), mercedes@iq.unesp.br (H.M. Villullas).

http://dx.doi.org/10.1016/j.apcatb.2017.10.037
Received 7 May 2017; Received in revised form 28 August 2017; Accepted 13 October 2017
Available online 18 October 2017
0926-3373/

considered as the most promising electrocatalysts for anodes of ADEFCs. A good understanding of the EOR reaction mechanism on such Pd-based catalysts and identifying the main intermediates and poisonous species formed under fuel cell continuous operation conditions are of critical importance in developing useful ADEFC technology. So far, reported results mostly address initial catalytic performances, while the stability of catalysts is seldom studied in fuel cells because long tests are required.

For Pd-based alloy catalysts, transition metal Ru is generally thought to enhance ethanol oxidation with the assistance of hydroxyl groups on the catalyst surface formed at lower potentials [13,14]. In a previous work carried out by Chen's group [17], the initial performance of Pd_xRu_y/C catalysts for the EOR was demonstrated to be better than that on Pd/C in ADEFC. Other studies also showed good EOR activities for PdRu/C as ADEFCs anodes [18]. Yet, the roles of Ru in PdRu/C and durability of PdRu/C catalysts for ethanol oxidation are still unclear.

In this work, we present a comprehensive study of Pd/C and Pd_2Ru/C catalysts aiming to unveil the roles of Ru and to determine the stability of the performance of ADEFC with Pd/C and Pd_2Ru/C anodes. Thus, activity for ethanol oxidation and stability were evaluated not only by half-cell testing, such as cyclic voltammetry (CV) and chronoamperometry (CA), but also by fuel cell testing under various test conditions. *In situ* FTIR experiments were also carried out to determine EOR intermediate and final products on Pd/C and Pd_2Ru/C as the function of varying electrode potentials.

2. Experimental

2.1. Catalyst preparation and characterization

Pd/C and Pd_2Ru/C (atomic ratio Pd:Ru 2:1) catalysts with 20 wt.% palladium loading were prepared by an impregnation method. A calculated amount of $PdCl_2$ (Alfa Aesar) and $RuCl_3$ (Santa Cruz Biotechnology) were dissolved in deionized water (Milli-Q) by adding 1.0 M HCl solution (Acros) and then mixed with Vulcan XC-72 carbon under vigorously stirring. A certain amount of sodium citrate (MP Biomedicals) was added into the suspension to act as a protective agent with 1:5 ratio of citrate to metals. The pH of the mixture was increased to over 12 by adding 1 M NaOH solution (Fisher Scientific, Inc.). Later, the mixture was heated to 80 °C and an excess of $NaBH_4$ solution was added dropwise to reduce the Pd and Ru precursors. After stirring for 12 h, the black suspension was filtered, washed with deionized water and dried at room temperature to obtain the Pd/C and Pd_2Ru/C catalysts.

X-ray diffraction measurements were carried out in a PANalytical EMPYREAN diffractometer equipment using Cu Kα radiation (λ = 1.5406 Å). Data were collected in the 2θ range 20–90 at 5 degrees min^{-1}. The morphologies of the catalysts were studied using a JEOL JEM 3200FS transmission electron microscope operated at 300 KV. To probe the electronic structure of states above the Fermi level, X-ray absorption spectroscopy (XAS) experiments were carried out around the Pd L_3 edge (3.173 eV) at the Tender X-rays Spectroscopy beamline of the Brazilian Synchrotron Light Laboratory (LNLS). Measurements were performed as described elsewhere [46].

2.2. Electrochemical characterization

The catalyst ink was prepared by ultrasonically mixing 2.0 mg of catalyst with 10 μL of Nafion solution (Nafion polymer dried weight: 5%), 0.5 mL of ethanol and 0.5 mL of de-ionized water. To form the working electrode, 20 μL of the prepared catalyst ink was dropped on the surface of a glassy carbon disk (5.5 mm diameter). The electrochemical measurements were conducted on an 8-channel Solartron 1470 Potentiostat Cell Test System (Solartron Analytical) using a standard three-electrode cell with a graphite column serving as the counter electrode and a Hg/HgO/NaOH (1.0 M) electrode (0.98 V *vs.* NHE) as reference. Experiments were carried out in argon-saturated 1.0 M NaOH fresh-prepared solution with and without ethanol (1.0 M) or acetaldehyde (0.1 M). CO oxidation on catalysts was carried out in 1.0 M NaOH solution by purging CO gas.

2.3. In situ FTIR measurements

Electrochemical *in situ* FTIR reflection spectroscopy experiments were performed on a Nexus 8700 spectrometer (Nicolet) equipped with a liquid-nitrogen-cooled MCT-A detector. Measurements were carried out in a three-electrode IR cell. A thin layer of electrolyte was formed by pressing the working electrode against the ZnSe window. A platinized Pt foil was used as counter electrode and Hg/HgO/NaOH (1.0 M) as reference electrode. The catalyst suspension was prepared with 1.0 mg of catalyst and 1.0 mL of ethanol and water mixture (ethanol:-water = 1:1) and 10 μL of Nafion solution (5 wt.%). The catalyst layer was prepared by depositing 5 μL of the suspension on a glassy carbon disk (5 mm diameter) embedded in a Teflon holder. After drying in air, the electrode was washed with pure water and then it was introduced into a conventional three-compartment cell containing 1.0 M NaOH solution, where it was electrochemically cleaned by potential cycling between −0.86 and 0.2 V. After obtaining an unchanging CV curve, the electrode was transferred to a 1.0 M ethanol in 1.0 M NaOH solution to perform *in situ* FTIR measurements. Spectra were collected in multi-stepped FTIR spectroscopy (MS-FTIR). The resulting spectra are reported as the relative change in reflectivity (*ΔR/R)*, which is calculated as

$$\frac{\Delta R}{R} = \frac{R(E_S) - R(E_R)}{R(E_R)} \quad (1)$$

where $R(E_S)$ and $R(E_R)$ are the single-beam spectra collected at the sample potential E_S and at the reference potential E_R, respectively.

2.4. Tests in single alkaline direct ethanol fuel cell

Catalyst performances were also characterized by running several different tests in a single alkaline direct ethanol fuel cell. The membrane electrode assemblies (MEA) with an active electrode area of 4.6 cm^2 consisted of a catalyst coated membrane (CCM), a Ni foam (Hohsen Corp.) as the anode backing layer and a TGP-H-090 carbon paper (Toray) as the cathode backing layer. The anode catalyst ink was prepared by mixing 16 mg of catalyst (Pd/C or Pd_2Ru/C) with Nafion solution. The cathode catalyst ink was prepared by ultrasonicating 8 mg active carbon (BP2000, Cabot Corp.), 8 mg MnO_2 nano-rod catalyst, and the A4 ionomer (Tokuyama Co.). The catalyst/ionomer (Nafion or A4) weight ratio was 80:20 in the anode and in the cathode. After homogenizing by sonication, the inks were airbrushed onto a 6.25 cm^2 Tokuyama A201 membrane (Tokuyama Co.) to form a CCM. A fuel cell test system (Scribner Associates Model 850e) was used for controlling the cell temperature, cathode humidity, and O_2 flow rate. The temperature of the fuel cell was maintained with a tolerance of ± 0.2 °C. The anode solution flow rate was controlled with an ESI MP2 micro peristaltic pump (Elemental Scientific Inc.).

Fuel cell performance was tested at different temperatures. First, tests were carried out at 40 °C, 50 °C, 60 °C, and 70 °C with a fuel solution containing 0.1 M KOH and 2.0 M ethanol. Then, using a fuel with higher KOH concentration (1.0 M KOH and 2.0 M ethanol) further tests were conducted at 70 °C, 80 °C and 90 °C, respectively. Electrochemical impedances of fuel cells were tested by using an 8-channel Solartron 1470 cell tester. Impedance spectra were recorded by superimposing a 10 mV AC signal at the different cell voltages in the potentiostatic mode with frequencies ranging from 100 K to 0.1 Hz. In these experiments, fuel cells were discharged at 0.5 V, 0.4 V, 0.3 V and 0.2 V by using 1.0 M KOH + 2.0 M ethanol at 70 °C. Finally, accelerated stability tests were conducted by circulating 500 mL of 2.0 M ethanol and 1.0 M KOH solution through the anode compartment of the fuel cell at 2 mL min^{-1}.

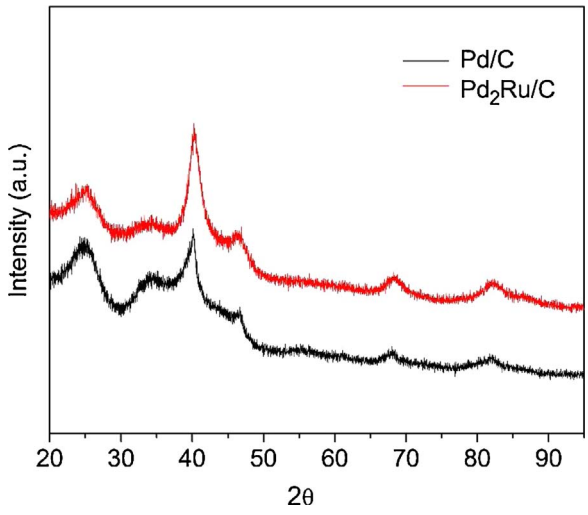

Fig. 1. X-ray diffraction patterns of Pd/C and Pd_2Ru/C catalysts.

The fuel cell temperature was maintained at 90 °C and O_2 was passed through the cathode at 0.1 L min^{-1}. A constant current of 100 mA cm^{-2} was discharged from the fuel cell until the voltage reached 0.1 V.

3. Results and discussion

XRD patterns of Pd/C and Pd_2Ru/C catalysts are shown in Fig. 1. The two catalysts showed patterns with a broad peak located around 25° belonging to the (002) plane of carbon with hexagonal structure. The diffraction pattern of Pd/C shows four peaks located around 40°, 47°, 68° and 82°, which are attributed to the (111), (200), (220), and (311) planes of the Pd face-centered cubic (fcc) structure (JCPDS 46-1043), respectively. The Pd_2Ru/C catalyst shows a pattern similar to that of Pd/C, but with the diffraction peaks slightly shifted to higher 2θ values. From the Pd (220) peak, the average crystallite size was calculated by Scherrer's equation as being 4.8 and 4.2 nm for Pd/C and Pd_2Ru/C, respectively. The lattice parameter calculated by Bragg's equation is 0.3905 nm for Pd/C and 0.3883 nm for Pd_2Ru/C. The shrinking of the lattice parameter reveals alloy formation between Pd and Ru due to the partial substitution of Pd by Ru, as expected from the smaller atomic radius of Ru (R_{Ru} = 1.34 Å < R_{Pd} = 1.37 Å). The diffraction peak around 33.6° is attributed to the (002) plane of tetragonal PdO (JCPDS 41-1107), which has been observed previously [17]. This peak was also observed in the diffraction pattern of Pd_2Ru/C. The TEM images of Pd/C and Pd_2Ru/C catalysts are shown in Fig. 2. Catalyst nanoparticles are uniformly dispersed on the carbon support and have an average size around 4 nm, which is consistent with the crystallite size obtained from XRD data.

When a transition metal absorbs X-rays, 2p electrons are excited to unfilled d orbitals (4d orbitals for second-row transition metals) resulting in an absorption peak known as absorption edge. The X-ray absorption spectra measured around the Pd L_3 edge (3173 eV, $2p_{3/2} \rightarrow$ d transitions) for Pd/C and Pd_2Ru/C are depicted in Fig. 3, where the absorption peak region is shown enlarged in the inset. Spectra shown were normalized using with the ATHENA program [48]. Clearly, the intensity of the absorption peak is considerably higher for Pd_2Ru/C evidencing a larger electronic vacancy of the Pd 4d band than for Pd/C. These results are in agreement with what were reported for PtRu materials, which show that the presence of Ru (metallic or oxidized) promotes an increase in the Pt 5d band vacancy [49].

Fig. 4 shows the cyclic voltammograms (CV) of Pd/C and Pd_2Ru/C recorded in argon-saturated 1.0 M NaOH solution. The Pd/C catalyst shows a typical CV curve in alkaline media. During the forward potential scan, it is observed that OH adsorption starts immediately after

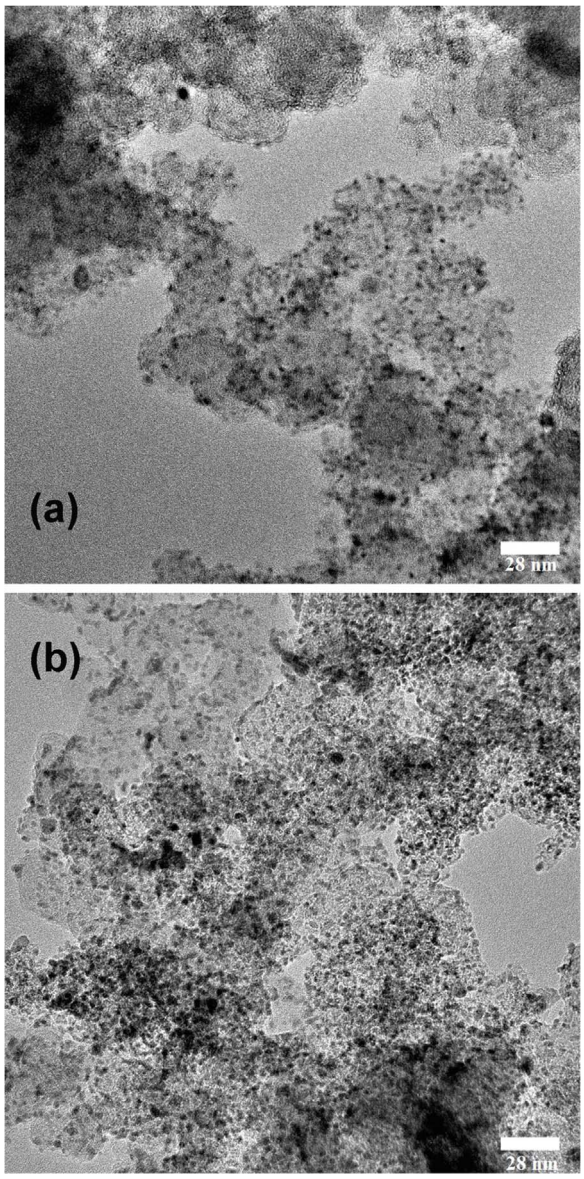

Fig. 2. TEM images of (a) Pd/C and (b) Pd2Ru/C.

the hydrogen desorption peak observed at −0.34 V, and then, Pd is gradually oxidized. In the backward potential scan, the current peak corresponding to the reduction of Pd oxides and the adsorption of hydrogen at more negative potentials are observed. The CV curve of Pd_2Ru/C is quite different from the Pd/C: a broad double-layer region associated to the pseudo-capacitive contribution of Ru to the double layer charging [50] indicates the presence of Ru on the surface of the nanoparticles and/or segregated, which is consistent with the XRD results. A current peak of OH adsorption is not obvious on the Pd_2Ru/C. As indicated by the XAS measurements that the electronic vacancy of the Pd 4d band is higher for Pd_2Ru/C than for Pd/C, OH adsorption on Pd sites is expected to start at lower potentials for Pd_2Ru/C than Pd/C, and to be close to the desorption of hydrogen. If OH adsorption on Pd begins at lower potentials, a shift in the same direction can be expected for the onset potential of PdO formation. In the backward potential scan, the PdO reduction process seems to merge with the pseudo-capacitive contribution of Ru. In Fig. 4, the PdO reduction peak is shifted toward lower potentials, which could correspond to the reduction of a somewhat thicker PdO layer [51], which is formed on the Pd_2Ru/C catalyst.

The electrocatalytic activities of EOR on Pd_2Ru/C and Pd/C

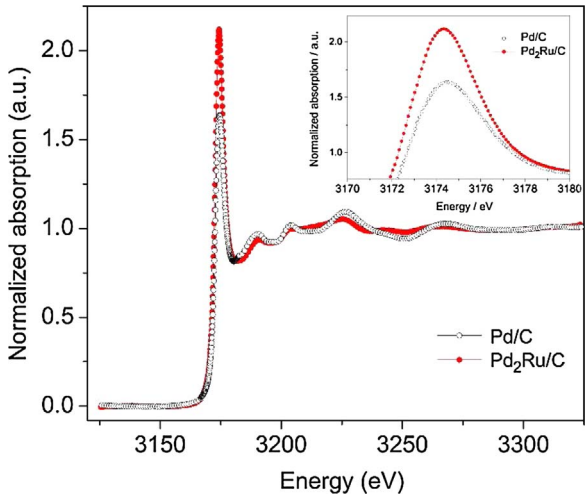

Fig. 3. CV curves of Pd/C and Pd_2Ru/C catalysts in argon-saturated 1.0 M NaOH solution. Scan rate: 20 mV s^{-1}. Room temperature. Comparison of X-ray absorption spectra for Pd/C and Pd2Ru/C taken around Pd L3 adsorption edge. Insert: region of adsorption peak enlarged.

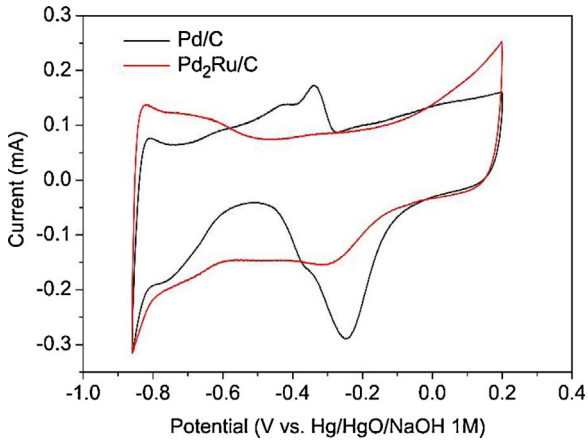

Fig. 4. Comparison of X-ray absorption spectra for Pd/C and Pd_2Ru/C taken around the Pd L3 adsorption edge. Inset: region of absorption peak enlarged. CV curves of Pd/C and Pd2Ru/C catalysts in Ar-saturated 1.0 M NaOH solution. Scan rate: 20 mV s^{-1}. Room temperature.

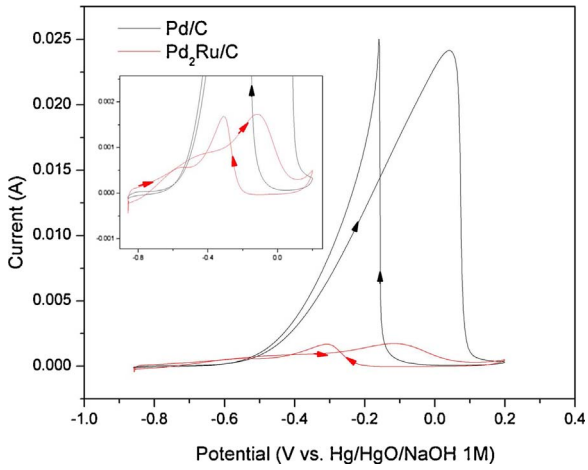

Fig. 5. CV curves of Pd/C and Pd_2Ru/C catalysts in 1.0 M NaOH + 1.0 M ethanol. Scan rate: 20 mV s^{-1}. Room temperature.

catalysts were studied by conventional CV measurements in 1.0 M NaOH solutions containing 1.0 M ethanol. As shown in Fig. 5, during the positive scan, ethanol oxidation on Pd/C begins at about −0.6 V, while an oxidation peak appears at around 0.04 V. As potential is further increased, the ethanol oxidation current drops rapidly due to the formation of Pd oxide. In the negative scan, as soon as the reduction of Pd oxides occurs and metallic Pd sites are gradually recovered, ethanol is oxidized on the fresh Pd surface. In contrast, for the Pd_2Ru/C catalyst, two-oxidation processes appear in both positive and negative potential scans. The current begins to increase at much lower potential (about −0.8 V) defining a shoulder that goes to about −0.40 V followed by the main ethanol oxidation peak observed around −0.10 V, which agree with the earlier work [17] that showed Pd_xRu_y/C catalysts having lower EOR onset potential and lower peak potential than the Pd/C. Also it is worth to point out that EOR currents obtained on Pd_2Ru/C are an order smaller than that on Pd/C.

Currently, it is well accepted that ethanol oxidation takes place through parallel pathways. In the so-called C2 pathway, the C—C bond is not broken, while ethanol is first oxidized to acetaldehyde that is further oxidized to acetic acid (or acetate in alkaline solution):

$$CH_3CH_2OH \rightarrow CH_3CH_2OH_{(ad)} \rightarrow CH_3CHO \rightarrow CH_3COOH \quad (2)$$

If the C—C bond is broken (C1 pathway), intermediate species such as CO and CH_x fragments are produced, which can be further oxidized to CO_2 (or carbonate in alkaline solution):

$$CH_3CH_2OH \rightarrow CH_3CH_2OH_{(ad)} \rightarrow CO_{(ad)}, CH_{x(ad)} \rightarrow CO_2 \quad (3)$$

CV curves showing more than one current wave observed for ethanol oxidation on Pt in acid medium were considered indication of the reaction proceeding via more than one faradaic process. The first process was believed to correspond to the oxidation of ethanol to acetaldehyde and the main current peak due to the oxidation of the species formed in the first process (acetaldehyde or of an intermediate formed from acetaldehyde) [12]. It was pointed out, however, that in acid as well as in alkaline solutions, CO_2 (or carbonate) and acetic acid (or acetate) could also be formed at low potentials and, therefore, the first oxidation process could not, in principle, be attributted only to the formation of acetaldehyde. Lai et al. [12] suggested that in alkaline medium the deprotonated form of hydrated acetaldehyde (CH_3CHOHO^-) is likely to be the main reactive species for acetaldehyde oxidation and that the EOR might take place by the reaction mechanism shown in Fig. 6.

Because acetaldehyde and CO are possible intermediate species formed in the EOR, we carried out further CV studies of acetaldehyde oxidation and CO oxidation on Pd_2Ru/C and Pd/C in alkaline medium. 5-cycle CV curves recorded for both catalysts in 1.0 M NaOH solutions containing 0.1 M acetaldehyde are shown in Fig. 7. One can see clearly that both the onset and peak potentials of acetaldehyde oxidation on Pd_2Ru/C are shifted positively relative to Pd/C, indicating that Ru in the Pd_2Ru/C hinders acetaldehyde oxidation reaction. From comparison of the CV curves of acetaldehyde oxidation (Fig. 7) with the CV curve of ethanol oxidation (Fig. 5) on Pd_2Ru/C, it is quite obvious that the onset potential of acetaldehyde oxidation (> −0.6 V) is more positive than that of ethanol oxidation (~ −0.8 V), indicating that acetaldehyde need higher energy to be oxidized on Pd_2Ru/C. In contrast, the onset potential of acetaldehyde oxidation on Pd/C is much more negative (~ −0.8 V) than for ethanol oxidation (~ −0.5 V) on Pd/C, implying that the acetaldehyde produced by EOR can be oxidized immediately on Pd/C. The positive shift in the onset potential and the smaller currents of acetaldehyde oxidation on Pd_2Ru/C are consistent with the deprotonated form of the hydrated molecule (CH_3CHOHO^-) being the reactive specie for acetaldehyde oxidation, as suggested by Lai et al. [12]. The X-ray absorption results discussed above (Fig. 3) evidence that the Pd 4d band is more vacant for Pd_2Ru/C and, therefore, the adsorption energy of CH_3CHOHO^- should be higher on

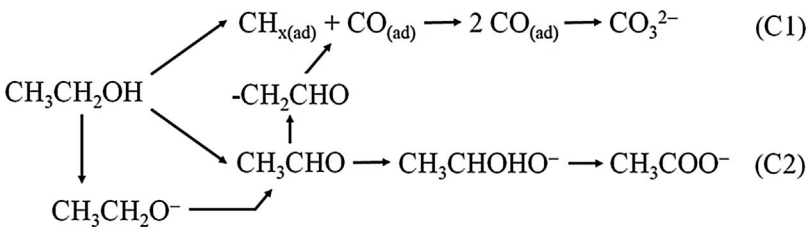

Fig. 6. EOR reaction scheme in solution of high pH, proposed by Lai et al. [12].

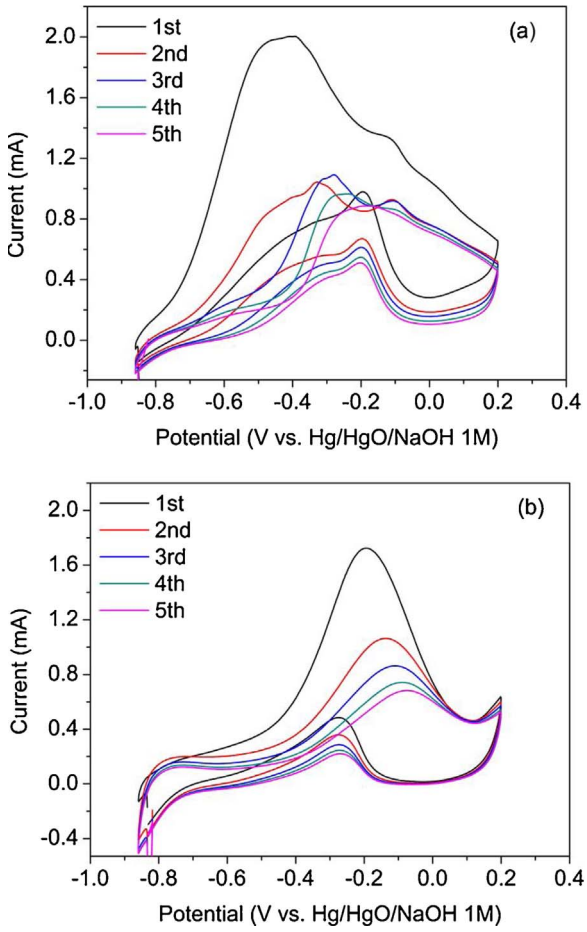

Fig. 7. CV curves of Pd/C (a) and Pd_2Ru/C (b) in 1.0 M NaOH + 0.1 M acetaldehyde. Scan rate: 20 mV s^{-1}. Room temperature.

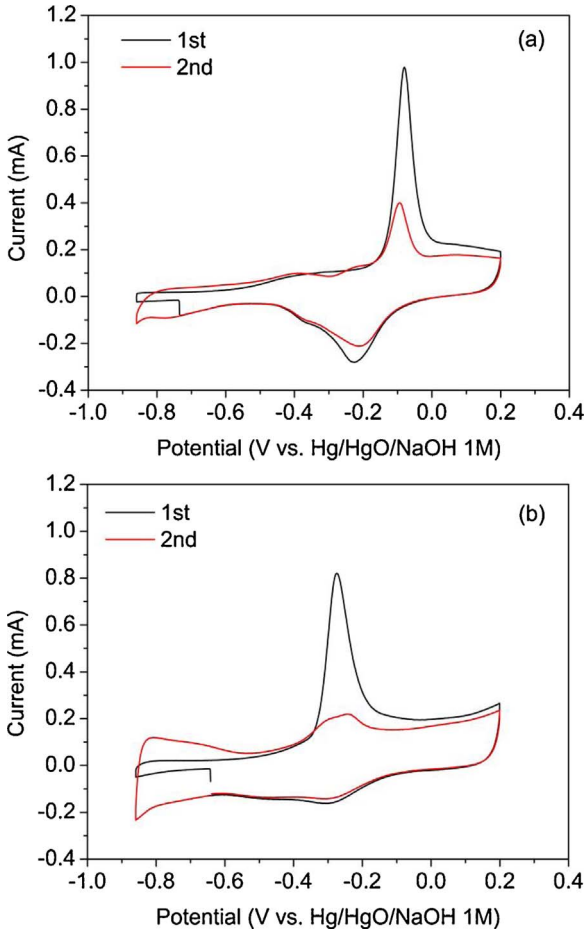

Fig. 8. CV curves of (a) Pd/C and (b) Pd_2Ru/C in CO-saturated 1.0 M NaOH. Scan rate: 20 mV s^{-1}. Room temperature.

Pd_2Ru/C, hindering its oxidation. In Fig. 7, it is also clear that both Pd_2Ru/C and Pd/C catalysts lost their electrocatalytic activities for acetaldehyde oxidation during cycling, suggesting that the species responsible for the deactivation are either products of acetaldehyde oxidation, which are formed on both catalysts, or species formed from acetaldehyde in solution. It is well known that the polymerization of acetaldehyde through an aldol condensation reaction is rather rapid in alkaline solutions. Since the CV curves shown in Fig. 7 were obtained in the solutions containing the same acetaldehyde concentration (0.1 M), the contents of the deprotonate form of hydrated acetaldehyde and of the dimer should be similar in the solution.

CO oxidation in alkaline solution was also investigated by purging CO gas in 1.0 M NaOH solution. As shown in Fig. 8, CO oxidation peak potential on Pd_2Ru/C is shifted negatively about 200 mV in comparison with that on Pd/C, indicating that the oxidation of CO species would be much easier on the Pd_2Ru/C catalyst than on the Pd/C.

Ethanol oxidation on Pd_2Ru/C and Pd/C catalysts was also studied by chronoamperometry (CA) measurements. The measured quasi-steady state currents of ethanol oxidation are shown in Fig. 9. For these experiments, the electrode potential was set at −0.476, −0.426 and −0.376 V, where the ethanol oxidation current was recorded for 15 min. Before stepping to the set potentials, the electrode was held at −0.86 V to make the initial redox state of the catalyst surface be identical for all the measurements. In Fig. 9, one can see that the currents for ethanol oxidation on Pd/C are much higher than those observed on Pd_2Ru/C at the same electrode potentials, in agreement with what was observed in the CV measurements (Fig. 5).

In situ FTIR spectroscopy measurements were carried out to identify the reaction products on Pd/C and Pd_2Ru/C catalysts. FTIR reference spectra were taken at −0.86 V, and studied spectra were recorded between −0.6 and 0.2 V *vs.* Hg/HgO/NaOH (1.0 M) with 0.1 V intervals in 1.0 M NaOH containing 1.0 M ethanol. The FTIR spectra for Pd/C and Pd_2Ru/C catalysts are depicted in Fig. 10. In both cases, two negative-going bands (gain bands) at 1553 and 1418 cm^{-1} [12,52–56] attributed to the symmetric and asymmetric stretching of the O—C—O bonds, respectively, are observed. These bands are assigned to acetate ions. The two positive-going bands (loss bands) observed at *c.a.* 1085 and 1045 cm^{-1} are attributed to the diminution of the amount of

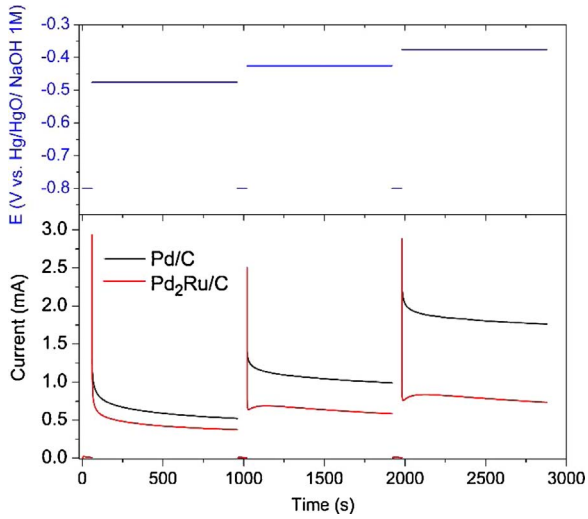

Fig. 9. Chronoamperometric profiles of Pd/C and Pd_2Ru/C in 1.0 M NaOH solution containing 1.0 M ethanol.

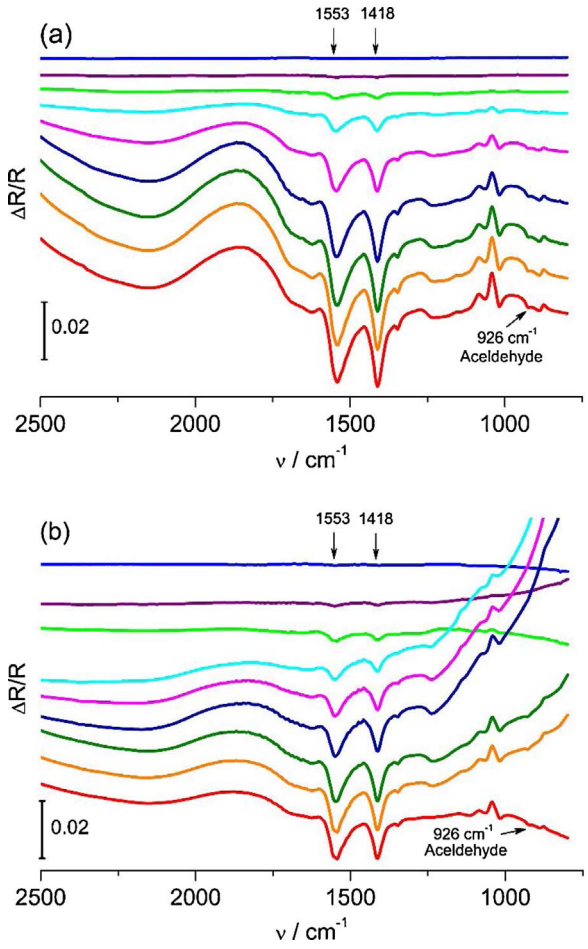

Fig. 10. *In situ* FTIR spectra of Pd/C (a) and Pd_2Ru/C (b) electrocatalysts, ES was varied from −0.60 to 0.20 V, ER = −0.86 V *vs.* Hg/HgO/NaOH(1.0 M), 400 scans, 8 cm^{-1}. 1.0 M ethanol in 1.0 M KOH. Each spectrum corresponds to an increase of 0.1 V compared to the previous one.

ethanol in the thin layer of electrolyte formed between the working electrode and the ZnSe optical window. The small gain band at about 926 cm^{-1} is ascribed to the C—C—O asymmetric stretching of acetaldehyde [52]. It should be noted that for Pd_2Ru/C this band appears at lower potentials than for Pd/C, which is consistent with attributing the

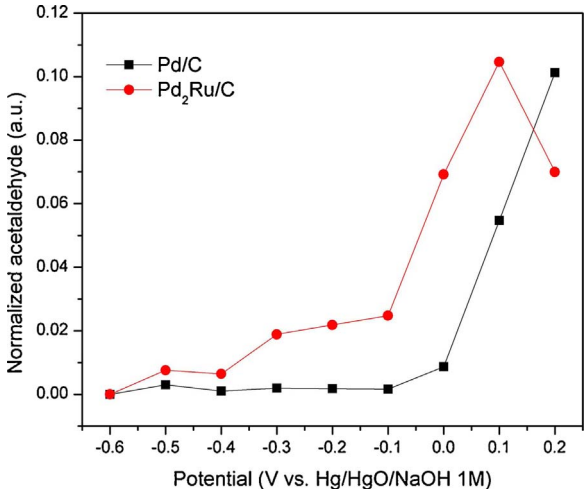

Fig. 11. Peak area of acetaldehyde band at 926 cm^{-1} normalized by ethanol oxidation current for the same amount of Pd loading *vs.* potential for Pd/C and Pd_2Ru/C catalysts.

EOR currents measured below −0.6 V in the CV curve (Fig. 5) mainly to the oxidation of ethanol to acetaldehyde. A CO_2 band (2343 cm^{-1}) is absent in both spectra. For the Pd/C catalyst, the lack of a CO_2 signal in the potential range of our studies is in agreement with the FTIR results for Pd black reported by Zhou et al. [55]. It should also be noted that spectra of Fig. 10 do not show evidence of the presence of linearly bonded CO (2055–2060 cm^{-1}) [53].

It should be pointed out here that the low absorptivity of acetaldehyde makes its detection quite challenging. The band around 926 cm^{-1} can be considered as a fingerprint for acetaldehyde, since it is the only acetaldehyde band that does not overlap with signals from other species [52,54]. An alternative way to analyze the effect of Ru on the production of acetaldehyde is to normalize the area of the acetaldehyde band by the ethanol oxidation current with the same Pd loading. Results are depicted in Fig. 11, which shows clearly that acetaldehyde production is considerably larger on Pd_2Ru/C than on Pd/C almost over the entire potential range in our measurements, except at the potential 0.2 V where Pd oxidation occurs on Pd_2Ru/C as shown in Fig. 4. Consequently, less acetaldehyde production was detected on Pd_2Ru/C than Pd/C at the potential of 0.2 V due to less Pd active sites available. Altogether, the FTIR results indicate that in alkaline solution ethanol oxidation on Pd/C and Pd_2Ru/C catalysts involves predominantly the production of acetaldehyde and acetate and occurs mainly via the pathway without C—C bond breaking.

It has been proposed that in alkaline solution the adsorption of ethanol would occur mainly through the oxygen atom (ethoxy species) [12,56]. The more vacant Pd 4d band of Pd_2Ru/C favoring the formation of ethoxy, which would be readily oxidized to acetaldehyde with the participation of oxygenated species provided by Ru, and would explain the EOR activity of Pd_2Ru/C at low potentials.

Finally, the EOR activity of Pd_2Ru/C and Pd/C were tested in ADEFCs that were assembled with identical cathodes, membrane (Tokuyamma A201), and ionomers, but varying anode catalysts (Pd_2Ru/C versus Pd/C). Experiments were conducted within two different temperature ranges (40–70 °C and 70–90 °C) and using two different feeding solutions (2.0 M ethanol in 0.1 M KOH and 2.0 M ethanol in 1.0 M KOH). Fig. 12 illustrates the polarization curves and power curves obtained with the ADEFCs under a wide range of test conditions. The initial performance of Pd_2Ru/C is much better than Pd/C, especially with the test solution of 2.0 M ethanol in 0.1 M KOH (Fig.12a). As the cell test temperature is raised, the performance of Pd_2Ru/C increases and continues to outperform Pd/C. However, the difference of maximal power capacity for the Pd_2Ru/C and Pd/C ADEFCs becomes less significant, especially when the strong alkaline fuel solution (2.0 M ethanol in 1.0 M KOH) is fed to the ADEFCs. The better initial fuel cell

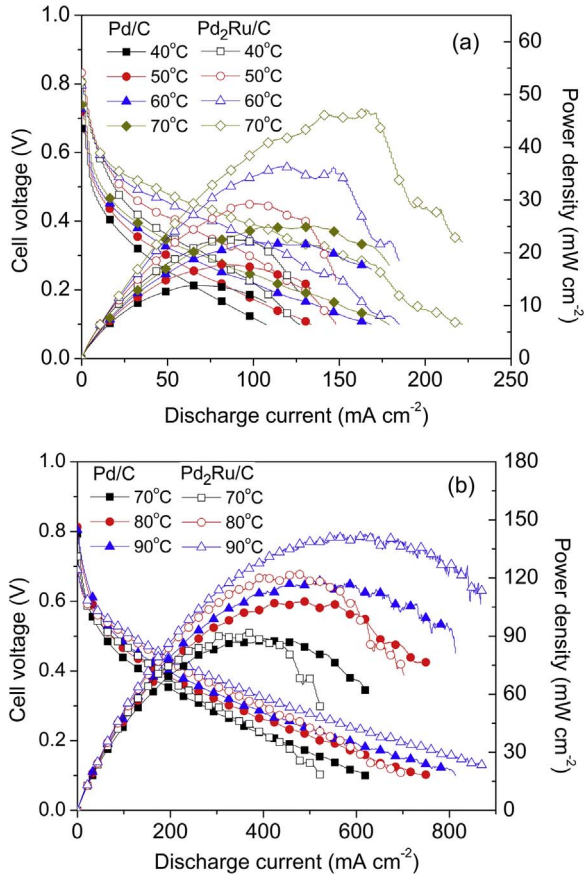

Fig. 12. Alkaline direct ethanol fuel cell performance. (a) Temperature range 40–70 °C and 0.1 M KOH + 2.0 M ethanol fuel solution. (b) Temperature range 70–90 °C and 1.0 M KOH + 2.0 M ethanol fuel solution.

performance with Pd_2Ru/C than Pd/C anode agrees with what was reported [17] but does not correlate directly to the CV and CA results. Since ADEFCs tests and CV measurements were carried out under different test conditions, it has been reported the catalysts with high catalytic activity observed by CV or CA measurements may perform poorly under the fuel cell test conditions, and vice versa [57,58]. Therefore, it is essential to conduct comprehensive studies not just using the half-cell CV and CA measurements but also the fuel cell testing in order to have a better understanding about the roles of Ru in Pd_2Ru/C for EOR.

To interpret the polarization behaviors of anodes with Pd_2Ru/C and Pd/C catalysts in ADEFCs, electrochemical impedance spectroscopy (EIS) measurements were also performed at 70 °C while discharging the ADEFC at various cell voltages (0.5, 0.4, 0.3 and 0.2 V) with 2.0 M ethanol in 1.0 M KOH feeding solution. Results are shown in Fig. 13, which shows that there is no reactant or product diffusion limitation, and the diameter of the semi-loop (the length between the high frequencies and low frequencies intersection points on the x-axis) can be attributed to the total (anode and cathode) charge transfer resistance. Because the cathodes are identical in all the test cells under the same tests conditions, the diameter of semi-loop of EIS can roughly correlate to the charge transfer resistance for ethanol oxidation at different cell voltage [59]. As shown in Fig. 13a, at cell voltage of 0.5 V, the charge transfer resistance on the Pd_2Ru/C is lower than that on Pd/C, and shrinks to the same size or becomes slightly larger than those on Pd/C at 0.4, 0.3 and 0.2 V, respectively. The decrease of the semi-loop diameter with the cell voltages is slower for Pd_2Ru/C than for Pd/C, indicating that the EOR activity on the Pd_2Ru/C becomes lower than that of Pd/C by lowering the cell voltages, which could be attributed, in principle, to the poisoning of the catalyst surface.

In order to further understand the influence and nature of the poisoning species, the durability tests of ADEFC with Pd_2Ru/C and Pd/C anodes were conducted by recording the cell voltage during continuously discharging the cell at a current density of 100 mA cm^{-2}. The alkaline fuel solution (2.0 M ethanol in 1.0 M KOH) was circulated during the run time test, which was terminated when the cell voltage dropped below 0.1 V. The results are depicted in Fig. 14 that shows the cell voltage decreasing gradually with time. This type of experiment is rarely performed because it could be very time-consuming, although such discharge curves would provide very valuable information on the stability of catalysts for ethanol oxidation. In Fig. 13, one can see that the run time of the ADEFC with Pd/C anode can reach 70 h, but only 10 h for Pd_2Ru/C anode under the same test conditions. In the initial 2.7 h, the cell voltage of the ADEFC with the Pd_2Ru/C anode is better than that with Pd/C. Then the cell voltage with Pd_2Ru/C anode drops steeply and shows a very poor performance in regard with that of Pd/C. The drop of the cell voltage can be understood by comparing the fuel solutions collected after the tests, as shown in Fig. 15. The fuel solution collected from that with Pd_2Ru/C anode is yellow, demonstrating that the formation of acetaldehyde in alkaline media leads to a high concentration of dimer. In a contrast, the solution collected with the Pd/C anode after 70 h test is only slightly yellowish, indicating a much lower concentration of the product of the aldol condensation reaction. This simple comparison of the collected fuel solutions helps us explain the rapid decrease of the performance of the ADEFC with Pd_2Ru/C anode, which had a much large amount of acetaldehyde produced and accumulated in the fuel solution that was circulated during the stability test, leading to formation of dimers that would block active sites of the catalyst surface. Similar observations were published for ethanol oxidation in alkaline solution on Pt electrodes, which lost EOR activity rapidly due to acetaldehyde and the dimer formation that adsorb on the Pt electrode surface and hinder the EOR [60].

In summary, the CV curves of ethanol oxidation (Fig. 5) and FTIR results (Figs. 10 and 11) show that acetaldehyde is formed on Pd_2Ru/C and Pd/C catalysts, but starting at lower potentials on Pd_2Ru/C. Results also reveal that although acetaldehyde formation is favored on Pd_2Ru/C, its oxidation is more difficult on this catalyst. The increase in the Pd 4d band electronic vacancy promoted by Ru allows explaining both observations. On Pd_2Ru/C the larger vacancy would favor ethanol adsorption through the oxygen atom and the ethoxy species formed would be readily oxidized to acetaldehyde with the participation of oxygenated species provided by Ru, while the delay in acetaldehyde oxidation would result from the stronger adsorption of CH_3CHOHO^-. Furthermore, we prove that although the initial ADEFC performance is better for the Pd_2Ru/C anode, the accumulation of acetaldehyde leads to larger amounts of polymerization products that block active sites and make the fuel cell discharge stability very poor (Fig. 14). Lastly, we demonstrate that accelerated fuel cell stability tests are essential for selecting anode catalysts for ADEFC applications.

Finally, it is important to point out that the performance degradation revealed by the accelerated fuel cell stability tests (Fig. 14) is not due to degradation of the anode material itself, but mainly to the blockage of reaction sites. Thus, the performance drop would occur to much lesser extent on a catalyst capable of oxidizing acetaldehyde (*i.e.*, oxidizing CH_3CHOHO^-) at a higher rate. The strength of adsorption of all adsorbed species involved in the EOR mechanism might be affected by the electronic properties of the catalyst. Therefore, finding out ways to reduce rapid drops of ADEFC performance is not an easy task. Detailed studies of the electronic occupancy of the Pd 4d band combined with the analysis of reaction products and intermediates, and accelerated fuel cell stability tests for other Pd-based catalyst will help to construct new rationales to determine the feasibility of their practical applications.

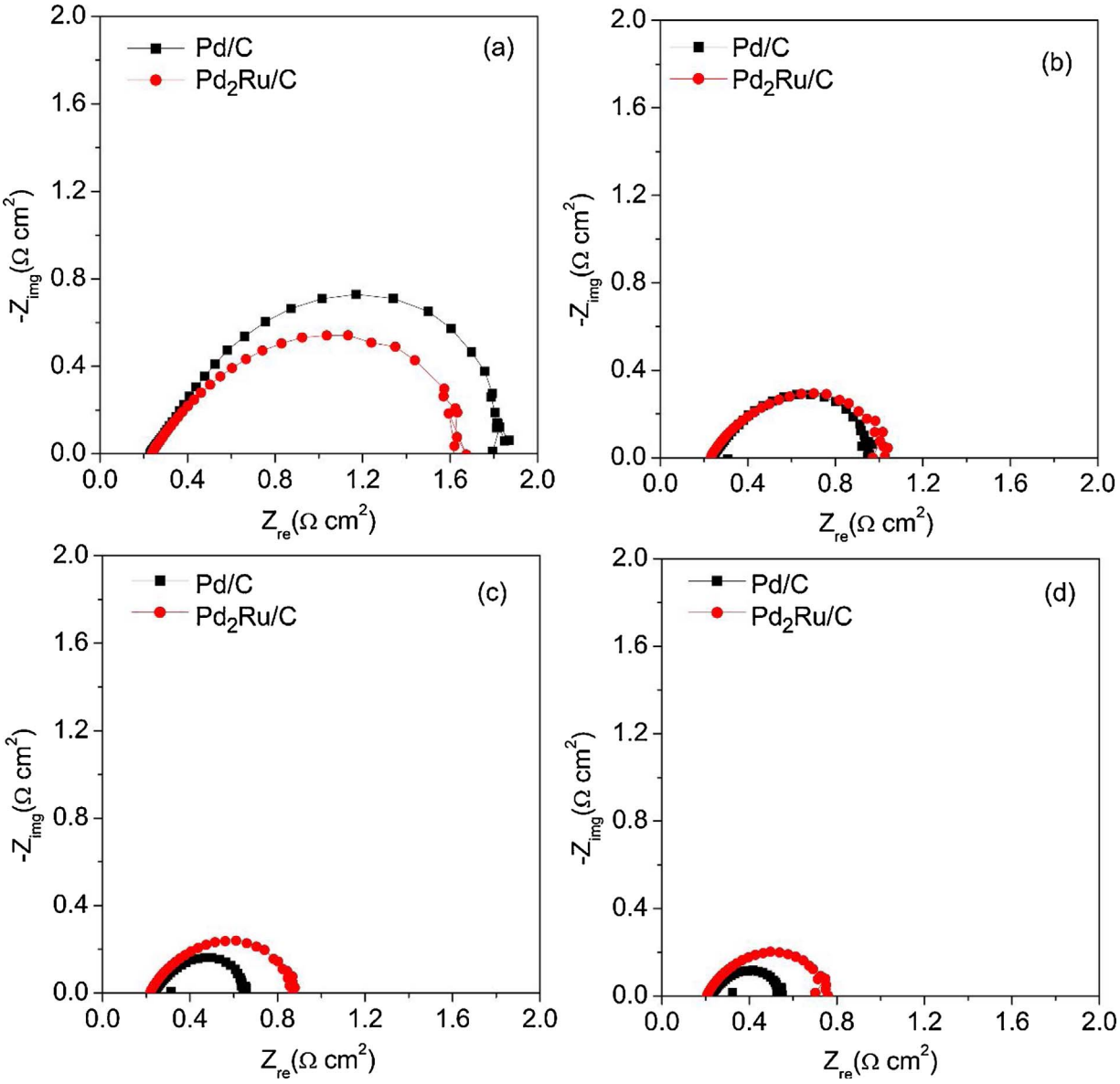

Fig. 13. Electrochemical impedance spectral of DEFC with Pd/C, Pd_2Ru/C anode catalysts at (a) 0.5, (b) 0.4, (c) 0.3 and (d) 0.2 V. Test temperature: 70 °C.

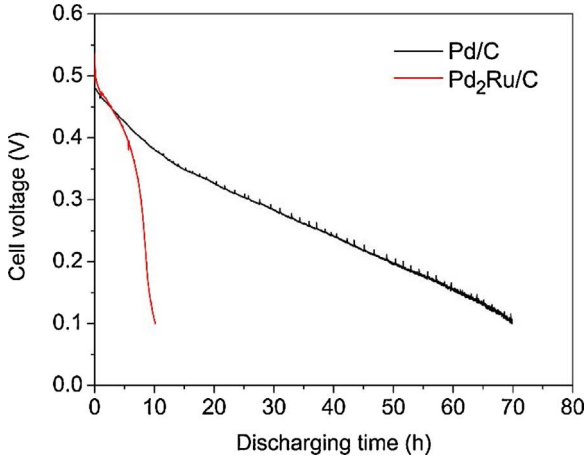

Fig. 14. Voltage *vs*. discharge time curves of alkaline direct ethanol fuel cell with Pd/C and Pd_2Ru/C anode catalysts. Test temperature: 90 °C. Feeding solution: Ethanol 2.0 M in 1.0 M KOH. Discharging current: 100 mA cm^{-2}.

4. Conclusions

In this paper, the electrocatalytic activity and stability of ethanol oxidation on Pd/C and Pd_2Ru/C were studied comprehensively by using cyclic voltammetry, chronoamperometry, *in situ* FTIR, single fuel cell test and electrochemical impedance spectroscopy measurements. CV curves of ethanol oxidation, acetaldehyde oxidation and CO oxidation in alkaline medium indicate that Ru in Pd_2Ru/C favors acetaldehyde formation and CO oxidation, but hinders acetaldehyde oxidation. The *in situ* FTIR data provide further evidence about the role of Ru in Pd_2Ru/C by favoring acetaldehyde formation in EOR. X-ray absorption data suggest that the Pd 4d band has a larger electronic vacancy for Pd_2Ru/C, which would favor ethoxy adsorption that can be readily oxidized to acetaldehyde with the participation of oxygenated species provided by Ru. At the same time, the larger vacancy might be responsible for hindering acetaldehyde oxidation. In consequence, larger amounts of acetaldehyde in the vicinity of the catalyst surface would lead to higher quantities of the dimer produced through the aldol condensation reaction. These species would strongly adsorb on the catalyst surface, blocking active sites for further ethanol oxidation. As the result, fuel cell performance drops much more rapidly on the

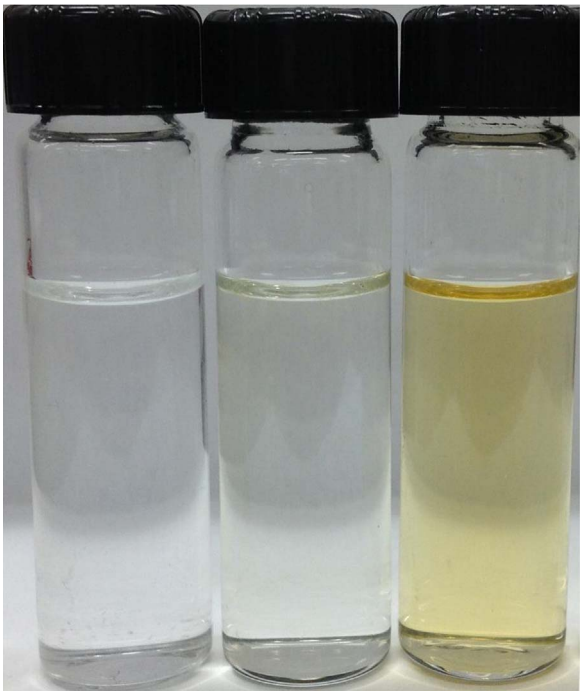

Fig. 15. Comparison of collected anode fuel solution after ADEFC durability tests. Freshly-prepared fuel solution (left) and fuel solution collected after the discharge experiments with Pd/C anode (center) and with Pd_2Ru/C anode (right).

Pd_2Ru/C anode than on the Pd/C in stability tests. These new insights of the roles of Ru in Pd_2Ru/C for EOR in alkaline media provide new grounds for selecting suitable anode catalysts for ADEFC applications.

Acknowledgements

We acknowledge collaborative financial support by National Science Foundation (NSF), United States of America (Contract 1402422), National Natural Science Foundation of China (NSFC), China (21361140374), and Fundação de Amparo à Pesquisa do Estado de São Paulo (FAPESP), Brazil (2013/50206-4; 2014/12255-6), as part of the International Union of Pure and Applied Chemistry (IUPAC) International Call on “Novel Molecular and Supramolecular Theory and Synthesis Approaches for Sustainable Catalysis”. Thanks are also due to the Brazilian Synchrotron Light Laboratory (LNLS) for assisting XAS experiments. This work was also partially supported by the US Army Research Office (grant W911NF-13-C-0062) and by CNPq, Brazil (407143/2013-0).

References

[1] M.Z.F. Kamarudin, S.K. Kamarudin, M.S. Masdar, W.R.W. Daud, Review direct ethanol fuel cells, Int. J. Hydrogen Energy 38 (2013) 9438–9453.
[2] Direct Alcohol Fuel Cells, in: H.R. Corti, E.R. Gonzalez (Eds.), Materials, Performance, Durability and Applications, Springer, Amsterdam, 2014.
[3] L. An, T.S. Zhao, Y.S. Li, Carbon-neutral sustainable energy technology: direct ethanol fuel cells, Renew. Sustain. Energy Rev. 50 (2015) 1462–1468.
[4] M.R. Tarasevich, O.V. Korchagin, A.V. Kuzov, Electrocatalysis of anodic oxidation of ethanol, Russ. Chem. Rev. 82 (2013) 1047–1065.
[5] L. Rao, Y.X. Jiang, B.W. Zhang, L.X. You, Z.H. Li, S.G. Sun, Electrocatalytic oxidation of ethanol, Prog. Chem. 26 (2014) 727–736.
[6] A. Brouzgou, S.Q. Song, P. Tsiakaras, Low and non-platinum electrocatalysts for PEMFCs: current status challenges and prospects, Appl. Catal. B: Environ. 127 (2012) 371–388.
[7] E. Antolini, E.R. Gonzalez, Alkaline direct alcohol fuel cells, J. Power Sources 195 (2010) 3431–3450.
[8] A. Brouzgou, A. Podias, P. Tsiakaras, PEMFCs and AEMFCs directly fed with ethanol: a current status comparative review, J. Appl. Electrochem. 43 (2013) 119–136.
[9] M.A.F. Akhairi, S.K. Kamarudin, Catalysts in direct ethanol fuel cell (DEFC): an overview, Int. J. Hydrogen Energy 41 (2016) 4214–4228.
[10] Y. Wang, S.Z. Zou, W.B. Cai, Recent advances on electro-oxidation of ethanol on Pt- and Pd-based catalysts: from reaction mechanisms to catalytic materials, Catalysts 5 (2015) 1507–1534.
[11] G. Tremiliosi-Filho, E.R. Gonzalez, A.J. Motheo, E.M. Belgsir, J.M. Leger, C. Lamy, Electro-oxidation of ethanol on gold: analysis of the reaction products and mechanism, J. Electroanal. Chem. 444 (1998) 31–39.
[12] S.C.S. Lai, S.E.F. Kleijn, F.T.Z. Ozturk, V.C.V. Vellinga, J. Koning, P. Rodriguez, M.T.M. Koper, Effects of electrolyte pH and composition on the ethanol electrooxidation reaction, Catal. Today 154 (2010) 92–104.
[13] O.A. Hazzazi, G.A. Attard, P.B. Wells, F.J. Vidal-Iglesias, M. Casadesus, Electrochemical characterisation of gold on Pt{h k l} for ethanol electrocatalysis, J. Electroanal. Chem. 625 (2009) 123–130.
[14] S. Beyhan, K. Uosaki, J.M. Feliu, E. Herrero, Electrochemical and in situ FTIR studies of ethanol adsorption and oxidation on gold single crystal electrodes in alkaline, J. Electroanal. Chem. 707 (2013) 89–94.
[15] Y.Q. Liang, Z.D. Cui, S.L. Zhu, Y. Liu, X.J. Yang, Silver nanoparticles supported on TiO2 nanotubes as active catalysts for ethanol oxidation, J. Catal. 278 (2011) 276–287.
[16] A.F.B. Barbosa, V.L. Oliveira, J. van Drunen, G. Tremiliosi, Ethanol electro-oxidation reaction using a polycrystalline nickel electrode in alkaline media: temperature influence and reaction mechanism, J. Electroanal. Chem. 746 (2015) 31–38.
[17] L. Ma, H. He, A. Hsu, R.R. Chen, PdRu/C catalysts for ethanol oxidation in anion-exchange membrane direct ethanol fuel cells, J. Power Sources 241 (2013) 696–702.
[18] S. Carrion-Satorre, M. Montiel, R. Escudero-Cid, J.L.G. Fierro, E. Fatas, P. Ocon, Performance of carbon-supported palladium and palladium ruthenium catalysts for alkaline membrane direct ethanol fuel cells, Int. J. Hydrogen Energy 41 (2016) 8954–8962.
[19] E.A. Monyoncho, S. Ntais, F. Soares, T.K. Woo, E.A. Baranova, Synergetic effect of palladium-ruthenium nanostructures for ethanol electrooxidation in alkaline media, J. Power Sources 287 (2015) 139–149.
[20] E.J. Lim, Y. Kim, S.M. Choi, S. Lee, Y. Noh, W.B. Kim, Binary PdM catalysts (M = Ru Sn, or Ir) over a reduced graphene oxide support for electro-oxidation of primary alcohols (methanol, ethanol, 1-propanol) under alkaline conditions, J. Mater. Chem. A 3 (2015) 5491–5500.
[21] D.R.M. Godoi, J. Perez, H.M. Villullas, Alloys and oxides on carbon-supported Pt-Sn electrocatalysts for ethanol oxidation, J. Power Sources 195 (2010) 3394–3401.
[22] L.P.R. Moraes, B.R. Matos, C. Radtke, E.I. Santiago, F.C. Fonseca, S.C. Amico, C.F. Malfatti, Synthesis and performance of palladium-based electrocatalysts in alkaline direct ethanol fuel cell, Int. J. Hydrogen Energy 41 (2016) 6457–6468.
[23] Q.G. He, B. Shyam, K. Macounova, P. Krtil, D. Ramaker, S. Mukerjee, Dramatically enhanced cleavage of the CC bond using an electrocatalytically coupled reaction, J. Am. Chem. Soc. 134 (2012) 8655–8661.
[24] X.Y. Liu, Y. Zhang, M.X. Gong, Y.W. Tang, T.H. Lu, Y. Chen, J.M. Lee, Facile synthesis of corallite-like Pt-Pd alloy nanostructures and their enhanced catalytic activity and stability for ethanol oxidation, J. Mater. Chem. A 2 (2014) 13840–13844.
[25] F. Matsumoto, Ethanol and methanol oxidation activity of PtPb, PtBi, and PtBi2 intermetallic compounds in alkaline media, Electrochemistry 80 (2012) 132–138.
[26] A.N. Geraldes, D.F. da Silva, E.S. Pino, J.C.M. da Silva, R.F.B. de Souza, P. Hammer, E.V. Spinace, A.O. Neto, M. Linardi, M.C. dos Santos, Ethanol electro-oxidation in an alkaline medium using Pd/C, Au/C and PdAu/C electrocatalysts prepared by electron beam irradiation, Electrochim. Acta 111 (2013) 455–465.
[27] Y.W. Lee, M. Kim, Y. Kim, S.W. Kang, J.H. Lee, S.W. Han, Synthesis and electrocatalytic activity of Au-Pd alloy nanodendrites for ethanol oxidation, J. Phys. Chem. C 114 (2010) 7689–7693.
[28] M.S. Ahmed, S. Jeon, Highly active graphene-supported NixPd100-x binary alloyed catalysts for electro-oxidation of ethanol in an alkaline media, ACS Catal. 4 (2014) 1830–1837.
[29] Z. Qi, H.R. Geng, X.G. Wang, C.C. Zhao, H. Ji, C. Zhang, J.L. Xu, Z.H. Zhang, Novel nanocrystalline PdNi alloy catalyst for methanol and ethanol electro-oxidation in alkaline media, J. Power Sources 196 (2011) 5823–5828.
[30] T. Maiyalagan, K. Scott, Performance of carbon nanofiber supported Pd-Ni catalysts for electro-oxidation of ethanol in alkaline medium, J. Power Sources 195 (2010) 5246–5251.
[31] S.Y. Shen, T.S. Zhao, J.B. Xu, Y.S. Li, Synthesis of PdNi catalysts for the oxidation of ethanol in alkaline direct ethanol fuel cells, J. Power Sources 195 (2010) 1001–1006.
[32] M.C. Oliveira, R. Rego, L.S. Fernandes, P.B. Tavares, Evaluation of the catalytic activity of Pd-Ag alloys on ethanol oxidation and oxygen reduction reactions in alkaline medium, J. Power Sources 196 (2011) 6092–6098.
[33] K. Kakaei, M. Dorraji, One-pot synthesis of Palladium Silver nanoparticles decorated reduced graphene oxide and their application for ethanol oxidation in alkaline media, Electrochim. Acta 143 (2014) 207–215.
[34] H.Y. Na, L. Zhang, H.X. Qiu, T. Wu, M.X. Chen, N. Yang, L.Z. Li, F.B. Xing, J.P. Gao, A two step method to synthesize palladium-copper nanoparticles on reduced graphene oxide and their extremely high electrocatalytic activity for the electrooxidation of methanol and ethanol, J. Power Sources 288 (2015) 160–167.
[35] A. Serov, T. Asset, M. Padilla, I. Matanovic, U. Martinez, A. Roy, K. Artyushkova, M. Chatenet, F. Maillard, D. Bayer, C. Cremers, P. Atanassov, Highly-active Pd-Cu electrocatalysts for oxidation of ubiquitous oxygenated fuels, Appl. Catal. B: Environ. 191 (2016) 76–85.
[36] F. Munoz, C. Hua, T. Kwong, L. Tran, T.Q. Nguyen, J.L. Haan, Palladium-copper electrocatalyst for the promotion of the electrochemical oxidation of polyalcohol fuels in the alkaline direct alcohol fuel cell, Appl. Catal. B: Environ. 174 (2015) 323–328.

[37] X. Zhao, J. Zhang, L.J. Wang, Z.L. Liu, W. Chen, PdxCu100-x networks: an active and durable electrocatalyst for ethanol oxidation in alkaline medium, J. Mater. Chem. A 2 (2014) 20933–20938.
[38] J.D. Cai, Y.Y. Huang, Y.L. Guo, Bi-modified Pd/C catalyst via irreversible adsorption and its catalytic activity for ethanol oxidation in alkaline medium, Electrochim. Acta 99 (2013) 22–29.
[39] Y.Y. Huang, J.D. Cai, Y.L. Guo, A high-efficiency microwave approach to synthesis of Bi-modified Pt nanoparticle catalysts for ethanol electro-oxidation in alkaline medium, Appl. Catal. B: Environ. 129 (2013) 549–555.
[40] H.Y. Jin, T.Y. Xiong, Y. Li, X. Xu, M.M. Li, Y. Wang, Improved electrocatalytic activity for ethanol oxidation by Pd@N-doped carbon from biomass, Chem. Commun. 50 (2014) 12637–12640.
[41] K. Wu, X.B. Mao, Y. Liang, Y. Chen, Y.W. Tang, Y.M. Zhou, J. Lin, C.N. Ma, T.H. Lu, Multiwalled carbon nanotubes supported palladium-phosphorus nanoparticles for ethanol electrooxidation in alkaline solution, J. Power Sources 219 (2012) 258–262.
[42] M.S. Ahmed, S. Jeon, Electrochemical activity evaluation of chemically damaged carbon nanotube with palladium nanoparticles for ethanol oxidation, J. Power Sources 282 (2015) 479–488.
[43] H. Hua, C.G. Hu, Z.H. Zhao, H. Liu, X. Xie, Y. Xi, Pt nanoparticles supported on submicrometer-sized TiO2 spheres for effective methanol and ethanol oxidation, Electrochim. Acta 105 (2013) 130–136.
[44] C.W. Xu, Z.Q. Tian, P.K. Shen, S.P. Jiang, Oxide (CeO2, NiO,Co(3)O(4)and Mn3O4)-promoted Pd/C electrocatalysts for alcohol electrooxidation in alkaline media, Electrochim. Acta 53 (2008) 2610–2618.
[45] D.R.M. Godoi, H.M. Villullas, F.C. Zhu, Y.X. Jiang, S.G. Sun, J.S. Guo, L.L. Sun, R.R. Chen, A comparative investigation of metal-support interactions on the catalytic activity of Pt nanoparticles for ethanol oxidation in alkaline medium, J. Power Sources 311 (2016) 81–90.
[46] G.M. Alvarenga, I.B. Coutinho Gallo, H.M. Villullas, Enhancement of ethanol oxidation on Pd nanoparticles supported on carbon-antimony tin oxide hybrids unveils the relevance of electronic effects, J. Catal. 348 (2017) 1–8.
[47] L. Ma, D. Chu, R.R. Chen, Comparison of ethanol electro-oxidation on Pt/C and Pd/C catalysts in alkaline media, Int. J. Hydrogen Energy 37 (2012) 11185–11194.
[48] B. Ravel, M. Newville, THENA, ARTEMIS, HEPHAESTUS: data analysis for Xray absorption spectroscopy using IFEFFIT, J. Synchrotron Radiat. 12 (2005) 537–541.
[49] D.R.M. Godoi, J. Perez, H.M. Villullas, Effects of alloyed and oxide phases on methanol oxidation of Pt-Ru/C nanocatalysts of the same particle size, J. Phys. Chem. C 113 (2009) 8518–8525.
[50] S. Trasatti, G. Buzzanca, Ruthenium dioxide: new interesting electrode material. Solid state structure and electrochemical behaviour, J. Electroanal. Chem. 29 (1971) A1- & .
[51] A.E. Bolzan, Phenomenological aspects related to the electrochemical-behavior of smooth palladium electrodes in alkaline-solutions, J. Electroanal. Chem. 380 (1995) 127–138.
[52] P. Gao, S.C. Chang, Z.H. Zhou, M.J. Weaver, Electrooxidation pathways of simple alcohols at platinum in pure nonaqueous and concentrated aqueous environments as studied by real-time FTIR spectroscopy, J. Electroanal. Chem. 272 (1989) 161–178.
[53] T. Iwasita, E. Pastor, A DEMS and FTIR spectroscopic investigation of adsorbed ethanol on polycrystalline platinum, Electrochim. Acta 39 (1994) 531–537.
[54] G.A. Camara, T. Iwasita, Parallel pathways of ethanol oxidation: the effect of ethanol concentration, J. Electroanal. Chem. 578 (2005) 315–321.
[55] Z.Y. Zhou, Q.A. Wang, J.L. Lin, N. Tian, S.G. Sun, In situ FTIR spectroscopic studies of electrooxidation of ethanol on Pd electrode in alkaline media, Electrochim. Acta 55 (2010) 7995–7999.
[56] P.A. Christensen, S.W.M. Jones, A. Hamnett, In situ FTIR studies of ethanol oxidation at polycrystalline Pt in alkaline solution, J. Phys. Chem. C 116 (2012) 24681–24689.
[57] S. Sun, M.C. Halseid, M. Heinen, Z. Jusys, R.J. Behm, Ethanol electrooxidation on a carbon-supported Pt catalyst at elevated temperature and pressure: a high-temperature/high-pressure DEMS study, J. Power Sources 190 (2009) 2–13.
[58] J.S. Guo, H. He, D. Chu, R.R. Chen, OH-binding effects on metallophthalocyanine catalysts for O-2 reduction reaction in anion exchange membrane fuel cells, Electrocatalysis 3 (2012) 252–264.
[59] J.S. Guo, J. Zhou, D. Chu, R.R. Chen, Tuning the electrochemical interface of Ag/C electrodes in alkaline media with metallophthalocyanine molecules, J. Phys. Chem. C 117 (2013) 4006–4017.
[60] C. Buso-Rogero, E. Herrero, J.M. Feliu, Ethanol oxidation on Pt single-crystal electrodes: surface-structure effects in alkaline medium, ChemPhysChem 15 (2014) 2019–2028.